Available online at www.sciencedirect.com
SCIENCE DIRECT®
Journal of Colloid and Interface Science 280 (2004) 289–298
Journal of Colloid and Interface Science
www.elsevier.com/locate/jcis

# Roughness models for particle adhesion

Sean Eichenlaub [a], Anne Gelb [b], Steve Beaudoin [c,*]

[a] *Department of Chemical and Materials Engineering, Arizona State University, Tempe, AZ 85287, USA*
[b] *Department of Mathematics and Statistics, Arizona State University, Tempe, AZ 85287, USA*
[c] *School of Chemical Engineering, Purdue University, Forney Hall of Chemical Engineering, 480 Stadium Mall Drive, West Lafayette, IN 47907-2100, USA*

Received 10 December 2003; accepted 4 August 2004

Available online 30 September 2004

**Abstract**

The effects of different surface roughness models on a previously developed van der Waals adhesion model were examined. The van der Waals adhesion model represented surface roughness with a distribution of hemispherical asperities. It was found that the constraints used to define the asperity distribution on the surface, which were determined from AFM scans, varied with scan size and thus were not constant for all surfaces examined. The greatest variation in these parameters occurred with materials that had large asperities or with materials where a large fraction of the surface was covered by asperities. These rough surfaces were modeled with fractals and also with a fast Fourier transform algorithm. When the model surfaces generated using the Fourier transforms are used in the adhesion model, the model accurately predicts the experimentally observed adhesion forces measured with the AFM.
© 2004 Elsevier Inc. All rights reserved.

*Keywords:* Particle adhesion; Surface roughness; Post-CMP cleaning; Fourier transform

## 1. Introduction

Adhesion of particles is extremely important in wafer cleaning in the semiconductor manufacturing industry. Contaminant particles as small as 0.03 µm in diameter can cause devices to fail and reduce yield. Currently, large amounts of water and consumables, such as cleaning chemicals and brushes, are used to remove particles from wafers. Improved understanding of how particles adhere to surfaces will enable optimal cleaning protocols to be developed so that less water and consumables can be used while still ensuring that all particles are removed from the surface. Predictions of the adhesion force between the particles and the wafer surface give the force that must be overcome to remove the particles, and can be used in cleaning models [1–3] to help optimize the wafer cleaning process.

In systems of interest to the integrated circuit industry, the van der Waals (vdW) dispersion forces and electrostatic double layer interactions are the dominant interaction forces in particle adhesion to wafers [4–7]. vdW forces dominate the interaction when the particles are in contact with the surface [4–7]. The roughness of the surface has a large effect on the adhesion force, and changing roughness can change the vdW interaction by up to several orders of magnitude [6–14]. Several different models have been developed to describe the effects of surface roughness on vdW and electrostatic interactions [4,6,9,13,14]. The model developed by Cooper et al. has been experimentally validated for several systems relevant to chemical-mechanical planarization (CMP) and post-CMP cleaning. It accounts for particle geometry and deformation in addition to roughness effects [5]. In this model, hemispheres represent asperities on the particle and wafer surface. To model roughness, a computational scheme is employed in which hemispheres of randomly selected size are placed at random locations on a simulated surface until the model surface has the same mean roughness height, the same standard deviation about the mean height, and the

* Corresponding author. Fax: +1-765-494-0805.
*E-mail address:* sbeaudoi@purdue.edu (S. Beaudoin).

0021-9797/$ – see front matter © 2004 Elsevier Inc. All rights reserved.
doi:10.1016/j.jcis.2004.08.017

same fractional surface coverage by asperities as the surface being simulated. When roughness is simulated in this fashion, the adhesion model developed by Cooper et al. [4–8], accurately predicts the adhesion force for a number of relatively smooth materials or surfaces. However, because surface roughness can have such a large effect on the adhesion force, errors introduced by modeling surface roughness with hemispheres will cause adhesion force predictions to be inaccurate in many cases. A number of authors have shown that one of the assumptions inherent in this model, that the surface is stationary, is not accurate for all surfaces [15–17]. If the surface were stationary then the measured parameters used to create the model surfaces would not change with the measured length scale of the surface. The parameters used to describe the surface include the average height of the asperities, the standard deviation of the asperity height, and the fractional coverage of the surface by the asperities, all of which are determined from topographical AFM scans. Since for some surfaces of interest, these measured parameters do vary with the size of the AFM scan, two new approaches to generating model surfaces were determined. In addition to model surfaces generated using hemispheres, as was done by Cooper et al. [4,6], model surfaces generated using fractals, and model surfaces generated using Fourier transforms were considered. This Fourier transform approach can either reproduce a surface exactly or generate random surfaces with the same statistical roughness parameters: average roughness height, deviation about the average roughness height, and fractional coverage of the surface by asperities, as the original surface.

To determine the best approach to describing the effect of roughness on adhesion, three mathematical surfaces—(1) roughness represented by hemispherical asperities, (2) roughness represented by fractals, and (3) roughness represented by Fourier transforms—were used in Cooper et al.'s adhesion model [4], and the adhesion force predictions found using each model surface were compared. Adhesion force predictions were also made by taking a direct surface map of particles and surfaces of interest using an AFM and using the resulting three-dimensional data set in the adhesion model. All of the predictions were validated against experimentally measured adhesion forces.

## 2. Theory

### 2.1. Adhesion model

To predict the adhesion between two materials a previously developed adhesion model was used [4–8]. In addition to the surface roughness of each material, there are several other parameters that must be measured and used in this model. These include the elastic modulus of the materials, which is measured using a nanoindentor, the geometry of the particle, which is determined by creating a 3D volume reconstruction of the particle from SEMs of the particle from various angles, and the Hamaker constant. In the adhesion model, two surfaces are generated, one representing the particle and one representing the surface to which it adheres, based on the roughness of both surfaces and the particle geometry. The two surfaces are brought into contact and the asperities in contact are deformed based on the elastic modulus and the applied load. The van der Waals forces are then integrated between the two surfaces, to give the adhesion force. The model is evaluated a number of times. Each time, two new surfaces are created, and due to the different possible orientations of surface roughness and of the particle with respect to the opposing surface, a distribution of predicted adhesion forces is seen.

### 2.2. Hemispherical asperities

Cooper et al.'s adhesion model uses hemispherical asperities to represent surface roughness [4–8] and has been experimentally validated for some of the systems of interest here, including alumina and polystyrene particles interacting with silicon dioxide and copper surfaces in both air and aqueous systems. The average height of the asperities and the variance of the height are determined using an AFM to make topographical maps of the surface, and then to measure the size of all the peaks in a cross section of the topographic scan. This is shown in Fig. 1, in which $h$ represents the height of an asperity. The cross sections are taken at 50 nm intervals. The fractional coverage of the surface is determined by averaging the fraction of each cross section covered by asperities. A mathematical model surface is then generated subject to these parameters. First a hemispherical asperity is generated with a radius that is randomly chosen from a normal distribution determined using the average asperity size and the variation of the average asperity size. The asperity is then placed on a flat surface at a randomly chosen location. The fractional coverage of the surface is then calculated and compared to the measured fractional coverage. If the simulated surface does not attain the same fractional coverage as the measured surface, then another asperity is generated and placed on the surface until the experimental fractional coverage is reached.

This model has the ability to generate a large number of surfaces very quickly. In addition, this model works well

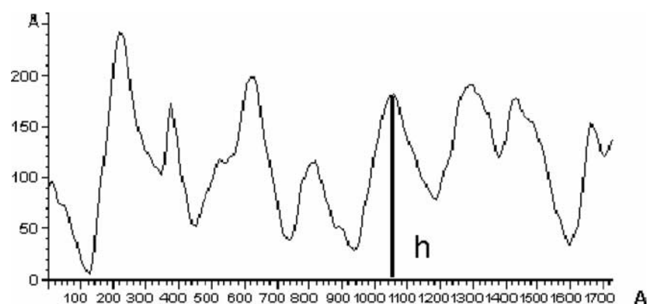


Fig. 1. Sample horizontal cross section taken from AFM scan of a copper surface.

when asperities are well defined, when the height/width ratio for the asperities is small, when the asperities are discrete (non-overlapping) and when they are easily distinguishable. If these conditions are met, this approach accurately represents the asperity layer. This may not be the case when the asperities have complex shapes, or if the roughness is due to a series of intersecting ridges instead of distinct asperities. In these cases the roughness parameters may vary with different scan lengths, and the volume of the asperity layer may be mis-estimated.

### 2.3. Fractal surfaces

A second method of generating mathematical models of rough surfaces is based on the use of fractals. Several authors have used fractals in developing an adhesion model between rough surfaces [16,18–20]. In these models, Mandelbrot's fractal geometry gives a mathematical model for many complex shapes which are invariant on different size scales [21–24]. A fractal surface is continuous, nondifferentiable, and possesses self-affinity. These properties are represented by the Weierstrass–Mandelbrot function, which is a superposition of sinusoids with geometrically spaced frequencies and amplitudes that follow a power law. The Weierstrass–Mandelbrot function is given by [23]

$$W(x) = \sum_{n=-\infty}^{\infty} \gamma^{-n(2-D)}\left(1 - e^{(i\gamma^n x)}\right)e^{(i\phi_n)}, \tag{1}$$

where $W$ is a complex function of the real variable $x$. The real portion of this equation can be used to find a fractal profile, $z(x)$.

$$z(x) = \sum_{n=-\infty}^{\infty} \gamma^{(D-2)}\left[\cos\phi_n - \cos(\gamma^n x + \phi_n)\right], \tag{2}$$

where $\gamma$ is a scaling variable that determines the density of the frequency spectrum, $\phi_n$ are phases that are randomly distributed between 0 and $2\pi$, and $D$ is the fractal dimension. $D$ in this case must be between 1 and 2. Equation (2) can be extended to two dimensions through [24]

$$z(\rho,\theta) = \left(\frac{\ln\gamma}{M}\right)^{1/2} \sum_{m=1}^{M} A_m \sum_{n=-\infty}^{\infty} (k\gamma^n)^{(D-3)} \times \left[\cos\phi_{m,n} - \cos\left(k\gamma^n \rho\cos(\theta - \alpha_m) + \phi_{m,n}\right)\right], \tag{3}$$

where $\rho$ and $\theta$ are polar coordinates. In this case, $A_m$ is the amplitude and can be chosen in a deterministic method or randomly. The anisotropy of the surface is controlled by the magnitude of $A_m$. If the surface is isotropic $A_m = A =$ a constant for all values of $m$, and if the surface is anisotropic, $A_m$ varies with $m$. In this application the surface is considered isotropic so only one value of $A_m$ is used. $\alpha_m$ is the angle corresponding to the direction of a corrugation of the surface and can also be chosen randomly, distributed between 0 and $\pi$, or distributed periodically by setting $\alpha_m = \pi m/M$, $k$ is a wavenumber that can be used to scale horizontal variability in the surface. The fractal dimension, $D$, now is between 2 and 3. Finally, $((\ln\gamma)^{1/2}/M^{1/2})$ is a normalizing factor.

If the surface is isotropic, then the fractal dimension of a surface profile, $D_p$, is related to the fractal dimension of a surface, $D_s$, by $D_s = D_p + 1$, and the surface and profile spectral densities are also related [20]. This allows such surfaces to be described by two parameters $D$ and $G$, as developed by Majumadar and Bhushan [20]. $G$ is a scaling coefficient, independent of frequency. For an isotropic surface, Yan et al. replaced the scale parameter $A$ in Eq. (3) with $A = 2\pi(2\pi/G)^{2-D}$ to derive the following form of Eq. (3) [25]

$$z(x,y) = L\left(\frac{L}{G}\right)^{D-2}\left(\frac{\ln\gamma}{M}\right)^{1/2} \sum_{m=1}^{M}\sum_{n=0}^{n_{\max}} \gamma^{(D-3)n} \times \left[\cos\phi_{m,n} - \cos\left(\frac{2\pi\gamma^n(x^2+y^2)^{1/2}}{L} \times \cos\left(\tan^{-t}\left(\frac{y}{x}\right) - \frac{\pi m}{M}\right) + \phi_{m,n}\right)\right]. \tag{4}$$

In this equation the wavenumber, $k$, is given by $k = 2\pi/L$, where $L$ is the length of the sample. The frequency index, $n$, has a lower limit of 0 and an upper limit of

$$n_{\max} = \operatorname{int}\left[\frac{\log(L/L_s)}{\log\gamma}\right], \tag{5}$$

where $L_s$ is smallest allowed length scale, approximately 0.4 nm.

If the surface can be represented by fractals, then the power spectrum and structure function of a surface that can be represented by Eq. (3) follow power laws given by

$$P(\omega) = \frac{G^{2(D-1)}}{\omega^{5-2D}} \tag{6}$$

and

$$S(\tau) = kG^{2(D-1)}\tau^{4-2D}, \tag{7}$$

where

$$k = \frac{\Gamma(2D-3)\sin((2D-3)\pi/2)}{2-D}. \tag{8}$$

If a surface can be characterized through the use of fractals, the plots of Eqs. (6) and (7) will be straight lines on a log–log plot and $D$ will remain constant at various length scales [26].

Fractals have been employed to characterize surface roughness in much the same way as has the value of the root mean square (RMS) roughness. A number of papers have discussed determining fractal parameters for use in comparing the roughness of two surfaces [27–31]. With the exception of the fractal dimension, $D$, and the fractal roughness, $G$, other parameters in Eq. (3), such as $\gamma$, are difficult to determine and must be assumed. This will affect the flatness of the model surface.

### 2.4. Fourier transforms

The final approach to describe surface roughness involves taking the Fourier transform of an AFM scan of the surface of interest. The essence of the Fourier transform of a waveform is to decompose or separate the waveform into a sum of sinusoids of different frequencies. If these sinusoids sum to the original waveform, then the sinusoids represent the Fourier transform of the original wave function [32]. The Fourier transform relationship is

$$Z(f) = \int_{-\infty}^{\infty} z(x) e^{-i2\pi f x} \, dx, \tag{9}$$

where $z(x)$ is the waveform to be decomposed into a sum of sinusoids and $Z(f)$ is the Fourier transform of $z(x)$. The discrete Fourier transform is similar to Eq. (9), but is evaluated at discrete points. It is given by

$$Z_k = \sum_{j=0}^{N-1} z(x_j) e^{-i2\pi f_k x_j}, \tag{10}$$

where $N$ is the number of data points. For a set of data in two dimensions, as shown in Fig. 1, the discrete Fourier coefficients for the data set are given by Eq. (10). The inverse discrete Fourier transform, used to transform the Fourier coefficients back into a dataset, is given by

$$z_x = \sum_{k=0}^{N} Z_k e^{i2\pi kx}. \tag{11}$$

Since the Fourier transform is a series of sine waves, the surface can be altered through the addition of a random phase $\phi_k$ [33,34]. If this is done, the surface will be slightly different than the original but will have the same statistical roughness parameters. With the addition of a random phase Eq. (11) becomes

$$z_x = \sum_{k=0}^{N-1} Z_k e^{i2\pi[\phi_k + kx/N]}. \tag{12}$$

In two dimensions Eq. (12) is given by

$$z_{x,y} = \sum_{k=0}^{M-1} \sum_{l=0}^{N-1} Z_{k,l} e^{i2\pi[\phi_{k,l} + kx/M + ly/N]}. \tag{13}$$

The fast Fourier transform can be used to compute the discrete Fourier transform. The fast Fourier transform is an algorithm which reduces the computing time of Eqs. (10) through (13) to time proportional to $N \log_2 N$ instead of $N^2$, where $N$ is the number of points to be described.

All three methods of describing surface roughness: hemispherical asperities, fractals and Fourier transforms, have advantages and disadvantages. All three may be useful in describing different types of surfaces.

## 3. Experimental

A Digital Instruments (DI) AFM was used to create topographical scans of three smooth surfaces (silicon dioxide, copper, and tungsten), and four rough surfaces (alumina, PTFE, copper, and tungsten). The three model surface generation techniques, the hemispherical asperity model, the fractal surface model and the Fourier transform model, were used to create model surfaces to describe the AFM scans. To create the hemispherical asperity model, the average asperity height, the standard deviation of the average height, and the fractional asperity coverage of the surface were determined from the AFM scan. To create the fractal surface the fractal dimension $D$ was determined from the AFM scans using the resident DI software. The fractal dimension was then used in Eq. (4) to create the surfaces. To generate the Fourier transform surface, the AFM scan is saved as an ASCII file and the list of surface heights is used in a mixed-radix fast Fourier transform algorithm [35]. Scans of four different sizes were made to determine if the scale affected the measured parameters or the model surfaces generated by each approach. The model surfaces were compared with direct surface topographical maps output from the AFM based on the linescans of the surfaces.

In a further test of the utility of the various approaches for generating model surfaces, adhesion forces between particles and surfaces in vacuum were measured using a Park Scientific AFM, and the adhesion was modeled using each roughness model in an existing vdW adhesion model [4,6]. The measured adhesion forces were compared to predictions made using the different model surfaces in the adhesion model. In addition to surface roughness the adhesion model accounts for the geometry of the particle and the surface to which it adheres as well as for the deformation of asperities on the particle and the surface. The amount of deformation that occurs is determined by the applied load and the bulk modulus of the particle and the surface, which is measured with a Hysitron nanoindentor. The particle geometry is characterized by taking SEMs of the particle mounted on the end of an AFM cantilever from 5 angles. These micrographs are then used in a commercially available three-dimensional volume reconstruction software package, *Photomodeler*. The Park Scientific AFM was operated in force mode to measure the adhesion force between the particles and surfaces of interest. The particles on the cantilevers were brought into and out of contact with the surfaces in a vacuum system. To ensure no effects of residual water, the samples were heated to 110 °C at a pressure of $1 \times 10^{-9}$ Torr and allowed to cool in vacuum before the measurements were made.

The predictions made with the adhesion model using each model surface were compared. The AFM scans also were used directly in the adhesion model, so that the model predictions using the exact surface maps would be available for comparison to the predictions when the different roughness models were used.

## 4. Results and discussion

Each roughness model was used to generate 1000 sets of model surfaces. Each set contained a roughness map of the particle and surface with which it interacted. This provided a statistical representation of the behavior of one particle interacting with a surface many times, or of a population of similar particles interacting with a population of similar surfaces.

### 4.1. Hemispherical asperities

Table 1 lists the roughness parameters for each of the materials studied. For the smooth surfaces such as silicon dioxide, the smooth copper sample and the smooth tungsten sample, modeling the asperities as hemispheres provided an adequate mathematical model surface. This is illustrated qualitatively in Fig. 2, which compares a three-dimensional view of the AFM scan of a silicon dioxide surface with the hemispherical asperity model of this surface. When the adhesion model was used to calculate the interaction force between 1000 silicon dioxide model surfaces interacting with 1000 smooth copper model surfaces, the histogram shown in Fig. 3 was created. The black points represent the predictions found using the model surfaces. The gray points represent the predictions found using the direct surface map from the AFM scan. There is good agreement between the two sets of predictions. The vertical lines represent the average and standard deviation of the adhesion force measured for this system with the ultrahigh vacuum AFM. There is good agreement between this measured adhesion force and both predictions.

Fig. 4 shows a comparison of the predicted forces found using the model surfaces (modeled using hemispheres) and the AFM surface maps for all of the systems examined. This figure shows that the model predictions made using the model surfaces accurately describe the average adhesion force and range of adhesion forces predicted with the direct surface maps from the AFM for the smooth surfaces (silicon dioxide, copper, and tungsten). However for the rough surfaces (alumina, rough copper, parylene, and PTFE), the predictions found with these model surfaces are not as accurate in determining the average adhesion force and range of adhesion forces. For these systems, the smooth surfaces have

Table 1
Hemispherical asperity parameters for each surface studied

| Material | Average asperity height (nm) | Standard deviation of asperity height (nN) | Fractional coverage (%) |
|---|---|---|---|
| Silicon dioxide | 1.3 | 0.7 | 38 |
| Tungsten | 0.8 | 0.3 | 82 |
| Alumina | 9.8 | 8.6 | 95 |
| Copper | 1.8 | 0.8 | 58 |
| Rough copper | 13.4 | 9.2 | 78 |
| PTFE | 280 | 185 | 97 |
| Parylene | 30 | 22 | 92 |

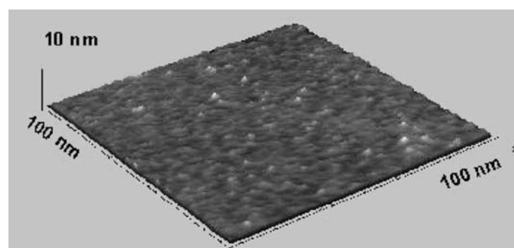


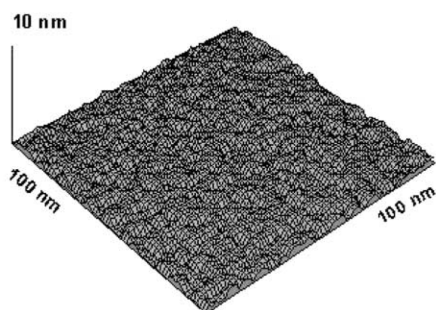


Fig. 2. Comparison of hemispherical asperity model surface and AFM scan of a silicon dioxide surface.

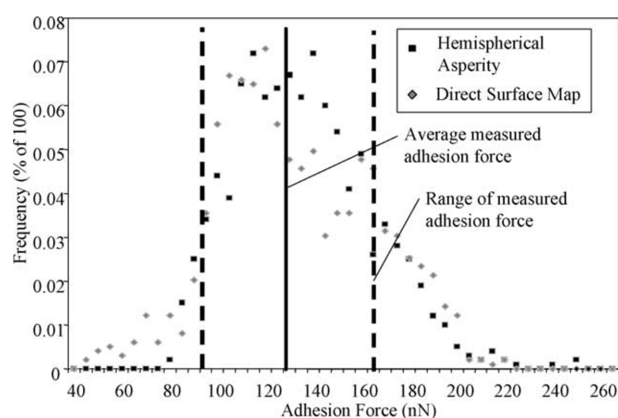


Fig. 3. Histogram of predicted adhesion forces calculated using hemispherical asperities and direct surface maps from the AFM, for the system of copper interacting with silicon dioxide. Also shown are the measured adhesion forces for this system.

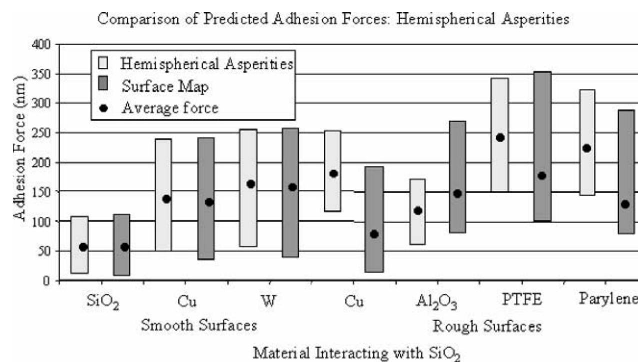


Fig. 4. Comparison of adhesion forces when predicted using hemispherical asperity model surfaces and using surface maps taken directly from AFM scan.

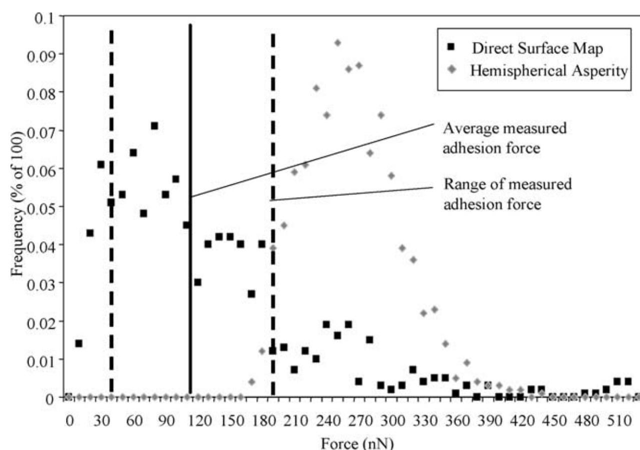


Fig. 5. Histogram of predicted adhesion forces for rough copper interacting with silicon dioxide. Predictions are made using hemispherical asperities and direct surface maps from the AFM. Also shown are the measured adhesion forces for this system.

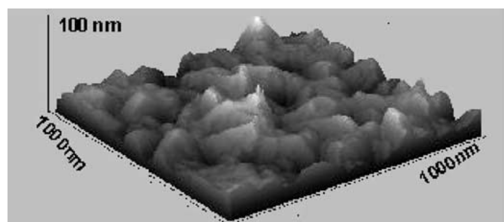


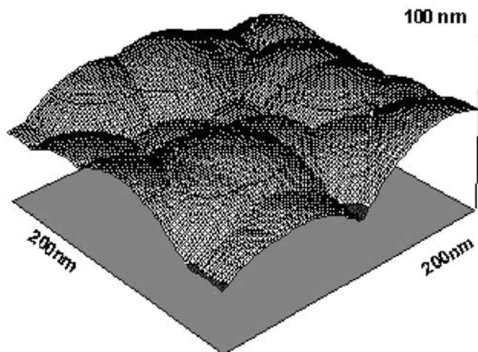


Fig. 6. AFM scan of rough PTFE surface and hemispherical asperity model of PTFE surface.

asperities that are smaller than 5 nm and cover less than 50% of the surface, while the rough surfaces have asperities that are larger than 15 nm and cover 70% of the surface or more. Fig. 5 shows a histogram of predicted adhesion force for one of these rough surfaces, the rough copper sample, interacting with silicon dioxide. Using hemispherical asperities to model surface roughness in this case overestimates the adhesion force. This is illustrated in Fig. 6, which shows how the use of hemispheres can overestimate the volume of interaction and create a smoother surface. The model surface has the same roughness characteristics (average roughness height, standard deviation about the mean height, and fractional coverage with asperities) as the AFM surface maps in

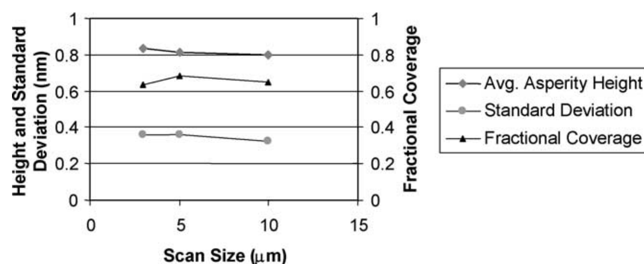


Fig. 7. Change of hemispherical asperity model parameters, average asperity height, standard deviation, and fractional coverage, with AFM scan size for silicon dioxide surfaces.

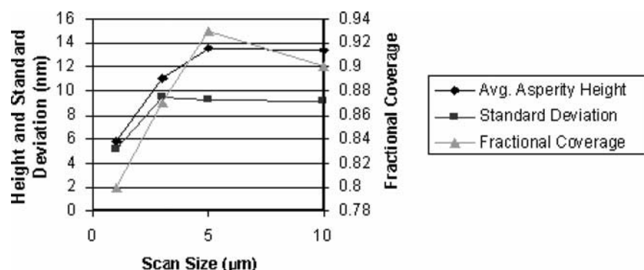


Fig. 8. Change of hemispherical asperity model parameters, average asperity height, standard deviation, and fractional coverage, with AFM scan size for rough copper surfaces.

this case, but the model surface appears much smoother than the surface measured with the AFM. When smooth surfaces interact, more mass from each surface can come into close proximity with the opposing surface, causing larger interaction forces to be generated.

There are several reasons that hemispheres cannot be used to create accurate models of the rough surfaces. First, the measured parameters, average asperity height, standard deviation of the asperity height and fractional coverage, may vary depending on scan size. This is shown in Figs. 7 and 8. Fig. 7 shows that for a smooth surface such as silicon dioxide, these parameters do not change appreciably with scan size. Fig. 8 shows that for a rough surface such as the rough copper surface, these parameters do vary with the size of the scan, making it difficult to determine the proper values of these parameters. Additionally, the roughness may have a given height but a much larger (or smaller) width, such that a spheroid would be a better model than a sphere. Finally, the roughness may be complex and cannot be modeled by spheres, such as would be the case for long intersecting ridges. These factors are related to the measured fractional coverage and the height of the asperities. Figs. 9 and 10 demonstrate the range over which the hemispherical asperity model will be appropriate. The fractional coverages and asperity heights shown in the plots are those from each surface considered. These surfaces included copper, silicon dioxide, parylene, PTFE, tungsten, and alumina, all interacting with silicon dioxide. Fig. 9 illustrates that when the fractional coverage becomes larger than 70% the hemispherical asperity model no longer accurately represents the actual surface. Each data point represents the absolute difference between

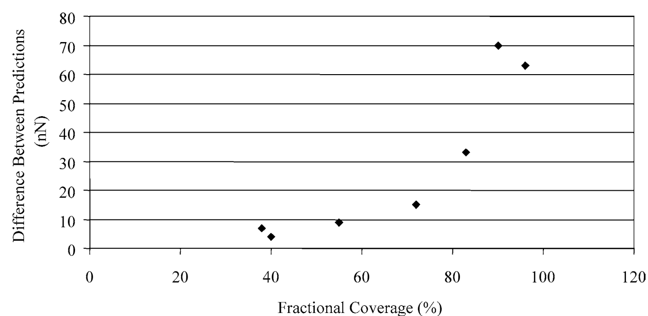


Fig. 9. Comparison of the difference between average adhesion forces predicted with the hemispherical asperity surface roughness model and the direct AFM surface map for surfaces with varying degrees of fractional asperity coverage.

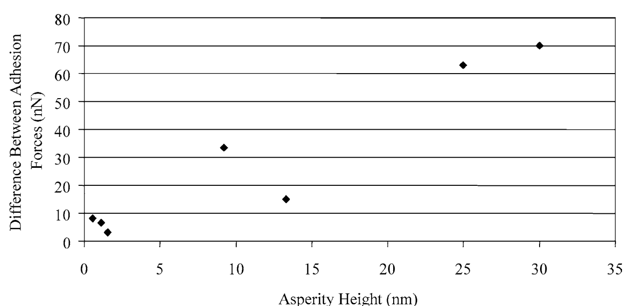


Fig. 10. Comparison of the difference between average adhesion forces predicted with the hemispherical asperity surface roughness model and the direct AFM surface map for surfaces with various average asperity heights.

the averages of the force predictions made with the model surface and the direct surface map from the AFM. The figure plots a data point for each of the systems studied. The interaction forces for silicon dioxide interacting with relatively smooth surfaces of copper (2 data points for 2 surfaces shown) and tungsten are plotted towards the left of the figure, and with relatively rough surfaces such as copper, alumina, PTFE, parylene, and tungsten, which have larger fractional coverages and are plotted toward the right of the figure. Fig. 10 is similar to Fig. 9 except that the asperity height is considered instead of the fractional coverage of the surface. The same systems are plotted as in Fig. 9 and the data points represent the same absolute difference of predicted average adhesion forces as in Fig. 9. Fig. 10 illustrates that once the height of the asperities becomes larger than approximately 15 nm the hemispherical asperity model cannot be used in the adhesion model to predict adhesion forces.

An example of a surface that exhibits these difficulties is shown in the AFM scan of the alumina surface in Fig. 11. The surface has three different roughness heights. There is an overall waviness to the surface, there are large grains, and finally there is small roughness distributed on these grains. The histogram in Fig. 12 shows that when the asperity heights are measured all three of these roughness scales contribute to the average. Specifically, the larger measured asperities correspond to the overall waviness of the surface, the medium sized measured asperities correspond to the larger grains of the surface roughness, and the smallest measured asperity heights correspond to the very small scale roughness present on each of the larger grains. As the scan size changes these affect the average and standard deviation. This surface is also almost completely covered with asperities indicating that the fractional coverage should be approximately 100%. When a fractional coverage of 100% is used, the model surface tends to be smoothed out because the asperities tend to overlap with each other, as shown in Fig. 6. Most of the traditional semiconductor surfaces will be more like the smooth surfaces than this alumina example. However, new materials such as polymer dielectrics, porous dielectrics, and organically-modified oxide dielectrics can be very rough.

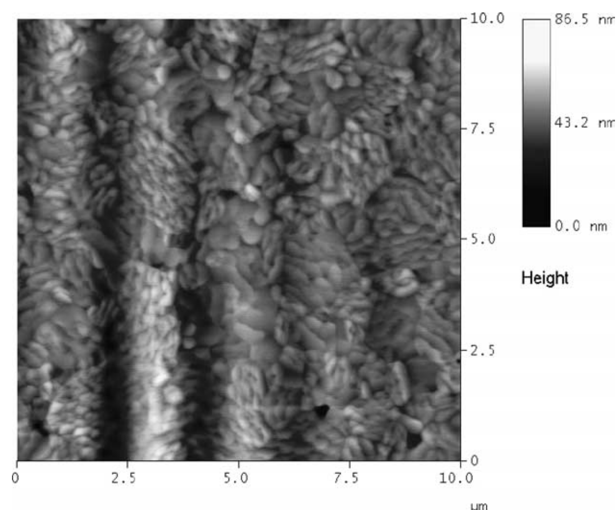


Fig. 11. AFM scan of alumina surface.

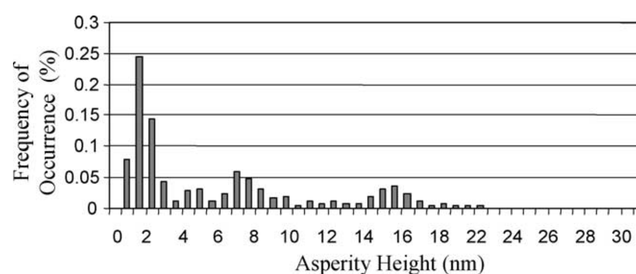


Fig. 12. Histogram of measured asperity heights for alumina surface.

### 4.2. Fractals

When fractals are used to create a model surface, the surfaces should have the same features on all length scales. When fractals were used to model the surfaces that were smooth, the silicon dioxide surface, the smooth copper surface, and the smooth tungsten surface, fractal dimensions of 2 were obtained. This made it very difficult to generate model surfaces that were representative of the different rough surfaces. Additionally, the power spectra in these cases did not follow the power law behavior of Eqs. (4) and (5). This was also true of the rough parylene surface, which had a fractal dimension of 2.001.

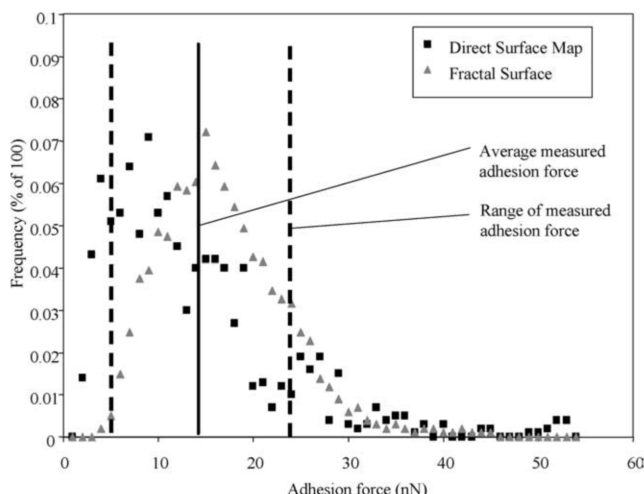


Fig. 13. Histogram of adhesion forces predicted with fractal surfaces compared with histogram of adhesion forces predicted using AFM surface maps for rough copper interacting with $SiO_2$.

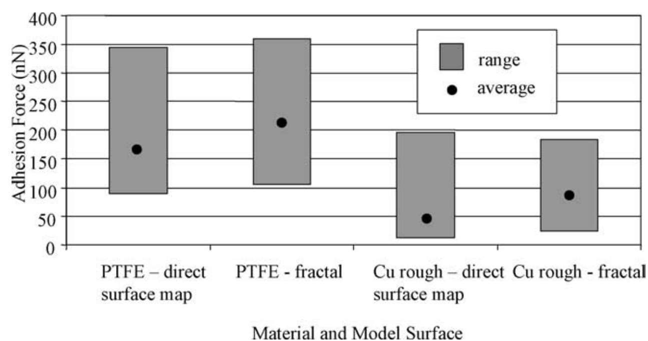


Fig. 14. Averages and ranges of adhesion forces predicted using fractal model surfaces and surface maps from AFM scans for PTFE and rough copper interacting with $SiO_2$.

Fractals were used to model the rough copper surface and the PTFE surface, which had fractal dimensions of 2.01 and 2.16. Fig. 13 shows a histogram comparing the predicted adhesion forces found using these model surfaces and the predicted forces found using the direct surface map when the rough copper was in contact with silicon dioxide. The agreement between the two sets of predictions is better than that obtained by using the hemispherical asperity model (shown in Fig. 7).

The predictions found using this model surface are still significantly different from the expected values. The same was true of the predictions made for the rough PTFE systems interacting with the silicon dioxide. In Fig. 14, the average and range of predicted adhesion forces for silicon dioxide interacting with the rough copper and PTFE are shown when the direct surface map and the fractal method are used to describe the roughness. This shows that the ranges of predicted interaction forces are in reasonable agreement when the fractals are used to describe the roughness, but the averages vary considerably. The fractal dimension should be unique and constant for a given sample at all scan lengths. However, in both of these cases the fractal dimension decreased with decreasing scan size, indicating that fractals should not be used to describe these surfaces.

### 4.3. Fourier transform

An example of a surface created with Eq. (13) in the FFT algorithm is shown in Fig. 15. It shows (A) the surface from the AFM surface map, (B) the surface recreated using FFT, and (C) a model surface after the addition of random phase angles.

Fig. 16 is a histogram, similar to the two shown in Figs. 5 and 13, comparing the predicted adhesion values found using the surface generated with FFT (and with a random phase angle in this case), and the predictions found using the direct AFM surface maps. In this case there is excellent agreement between the two sets of predictions. This is true of all the systems studied. Fig. 17 plots the maximum, minimum and average of the predictions for the rough copper and PTFE systems and compares the FFT model predictions with the predictions found using the direct AFM surface map. As can be seen, the agreement between the average predictions and the range of predicted forces are very good.

## 5. Conclusions

It is not possible to use a random distribution of ideal shapes to simulate surface roughness for all rough surfaces.

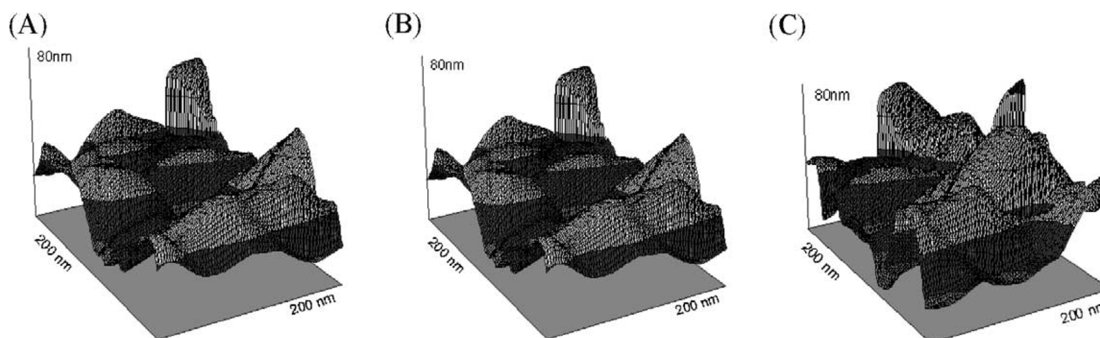


Fig. 15. (A) AFM scan of rough copper surface, (B) surface generated with FFT, and (C) surface generated with FFT and the addition of a random phase angle.

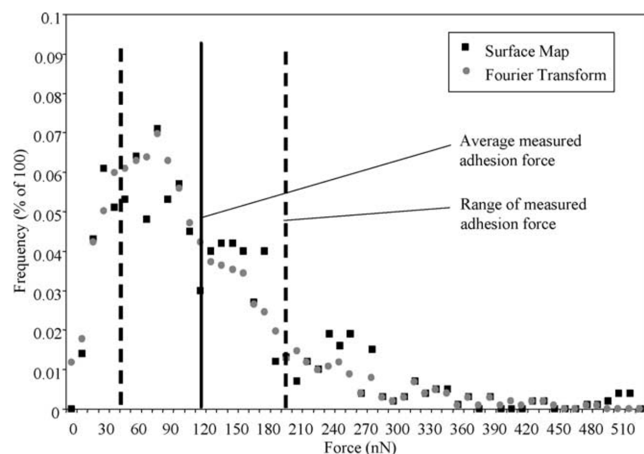


Fig. 16. Histogram of adhesion forces predicted with surfaces generated with Fourier transform compared with adhesion forces predicted with AFM surface maps for silicon dioxide interacting with rough copper.

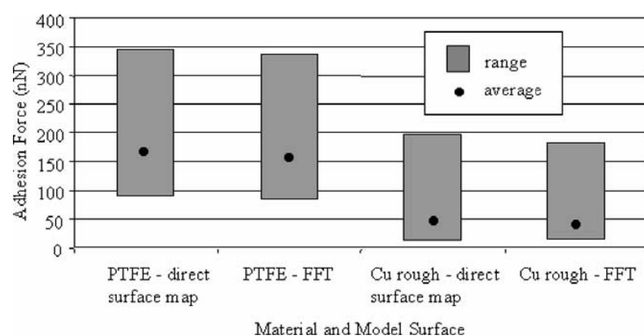


Fig. 17. Averages and ranges of adhesion forces predicted using Fourier transform model surfaces and surfaces from AFM scans.

Several constraints must be met in order for this approach to be effective. The fractional coverage of the surface by the asperities must be approximately 70% or less and the size of the asperities needs to be less than approximately 15 nm. If the coverage is larger, then it becomes difficult to distinguish between asperities, making it difficult to determine the roughness parameters accurately. This in turn makes it difficult to properly constrain the characteristics of the model asperities. Further, if the roughness takes the form of ridges or some other complex shape it is difficult to estimate the fractional coverage of the surface. Finally, the roughness parameters: asperity height, standard deviation, and fractional coverage, must remain constant at all length scales in order to create an accurate model surface using a distribution of ideal shapes. Otherwise, unique parameters cannot be found for a given surface. When the surface is basically smooth a random distribution of hemispheres is a fast way to generate a large number of accurate, simple model surfaces.

Fractal surfaces may be useful for a large number of engineering surfaces [16–20,24]. However they are not applicable to these semiconductor systems. For very smooth surfaces, typical of a semiconductor wafer, the fractal dimension in all cases was only slightly greater than 2, creating very little differentiation between the surfaces. For the rougher surfaces the fractal dimension was not constant at different length scales, indicating that the surface could not be characterized by fractals.

Finally, the Fourier transform can accurately reproduce any of the surfaces considered here. It is possible to reproduce a surface exactly, as well as to add a random phase angle to generate new model surfaces that have the same statistical roughness as the original surface, even though the roughness is distributed slightly differently.

## Acknowledgments

The authors are grateful for funding provided by the National Science Foundation (CAREER grant, CTS-9984620) and the National Science Foundation/Semiconductor Research Corporation Engineering Research Center for Environmentally Benign Semiconductor Manufacturing (EEC-9528813). The authors would also like to thank the Center for Solid State Electronics Research at Arizona State University for the use of their cleanroom and equipment, The Center for Interactive Nano-Visualization in Science and Engineering Education at Arizona State University for the use of their AFMs, and Michael Kozicki at Arizona State University for the use of his ultra-high vacuum AFM.

## References

[1] G. Burdick, N. Berman, S. Beaudoin, J. Electrochem. Soc. (2003), in press.
[2] G.M. Burdick, N. Berman, S. Beaudoin, J. Electrochem. Soc. (2003), in press.
[3] G.M. Burdick, N.S. Berman, S.P. Beaudoin, J. Nanoparticle Res. 3 (2001) 455.
[4] K. Cooper, A. Gupta, S. Beaudoin, J. Colloid Interface Sci. 234 (2001) 284.
[5] K. Cooper, S. Eichenlaub, A. Gupta, S. Beaudoin, J. Electrochem. Soc. 149 (2002) G239.
[6] K. Cooper, A. Gupta, S. Beaudoin, J. Electrochem. Soc. 148 (2001) G662.
[7] K. Cooper, N. Ohler, A. Gupta, S. Beaudoin, J. Colloid Interface Sci. 222 (2000) 63.
[8] K. Cooper, A. Gupta, S. Beaudoin, J. Colloid Interface Sci. 228 (2000) 213.
[9] S. Ning, J.Y. Walz, J. Colloid Interface Sci. 234 (2001) 90.
[10] L. Suresh, J.Y. Walz, J. Colloid Interface Sci. 183 (1996) 199.
[11] J.Y. Walz, Adv. Colloid Interface Sci. 74 (1998) 119.
[12] K.N.G. Fuller, D.F.R.S. Tabor, Proc. Royal Soc. London A 345 (1975) 327.
[13] J.L.M.J. van Bree, J.A. Poulis, B.J. Verhaar, Physica 78 (1974) 187.
[14] S. Bhattacharjee, C.-H. Ko, M. Elimelech, Langmuir 14 (1998) 3365.
[15] R.S. Sayles, T.R. Thomas, Nature 271 (1978) 431.
[16] K. Komvopoulos, W. Yan, Trans. ASME 120 (1998) 808.
[17] A. Majumadar, J. Tribology 112 (1990) 205.
[18] K. Komvopoulos, Wear 200 (1996) 305.
[19] K. Komvopoulos, W. Yan, J. Tribology 119 (1997) 391.
[20] A. Majumdar, B. Bhushan, J. Tribology 112 (1990) 205.
[21] A.P. Pentland, IEEE Trans. Pattern Anal. Machine Intell. 6 (1984) 661.
[22] R.F. Voss, Fundamental Algorithms Comp. Graph. F 17 (1985) 805.
[23] M.V. Berry, Z.V. Lewis, Proc. Royal Soc. London 370 (1980) 459.

[24] M. Ausloos, D.H. Berman, Proc. Royal Soc. London A 400 (1985) 331.
[25] W. Yan, K. Komvopoulos, J. Appl. Phys. 84 (1998) 3617.
[26] S. Ganti, B. Bhushan, Wear 180 (1995) 17.
[27] L. Lai, E.A. Irene, J. Vacuum Sci. Technol. B 17 (1999) 33.
[28] B. Dubuc, S.W. Zucker, C. Tricot, J.F. Quiniou, D. Wehbi, Proc. Royal Soc. London 425 (1989) 113.
[29] S. Chesters, H.Y. Wen, M. Lundin, G. Kasper, Appl. Surf. Sci. 40 (1989) 185.
[30] Q. Liu, L. Spanos, C. Zhao, E.A. Irene, J. Vacuum Sci. Technol. A 13 (1995) 1977.
[31] L. Spanos, E.A. Irene, J. Vacuum Sci. Technol. A 12 (1994) 2646.
[32] J.F. Price, Fourier Techniques and Applications, Plenum, New York, 1983.
[33] Y.Z. Hu, K. Tonder, Int. J. Machine Tools Manufact. 32 (1992) 83.
[34] J.-J. Wu, Tribology Int. 33 (2000) 47.
[35] E.W. Chu, Inside the Fft Black Box: Serial and Parallel Fast Fourier Transform Algorithms, CRC Press, Boca Raton, FL, 2000.